International Journal of Nanomedicine

Dovepress
open access to scientific and medical research

Open Access Full Text Article

ORIGINAL RESEARCH

Enhancing the Inhibition of Breast Cancer Growth Through Synergistic Modulation of the Tumor Microenvironment Using Combined Nano-Delivery Systems

Jingliang Wu[1,*], Qiao Lu[1,2,*], Jialin Zhao[3,*], Wendi Wu[3], Zhihua Wang[1], Guohua Yu[4], Guixiang Tian[2], Zhiqin Gao[2], Qing Wang[5]

[1]School of Medicine, Weifang University of Science and Technology, Weifang, 262700, People's Republic of China; [2]School of Life Science and Technology, Shandong Second Medical University, Weifang, 261053, People's Republic of China; [3]School of Clinical Medicine, Shandong Second Medical University, Weifang, 261053, People's Republic of China; [4]Department of Oncology, Weifang People's Hospital, Weifang, 261000, People's Republic of China; [5]Department of Stomatology, Weifang People's Hospital, Weifang, 261000, People's Republic of China

*These authors contributed equally to this work

Correspondence: Qing Wang, Department of Stomatology, Weifang People's Hospital, Weifang, 261000, People's Republic of China, Tel +86 158 6362 6389, Email wfwq8899@163.com

Purpose: Breast cancer is a prevalent malignancy among women worldwide, and malignancy is closely linked to the tumor microenvironment (TME). Here, we prepared mixed nano-sized formulations composed of pH-sensitive liposomes (Ber/Ru486@CLPs) and small-sized nano-micelles (Dox@CLGs). These liposomes and nano-micelles were modified by chondroitin sulfate (CS) to selectively target breast cancer cells.

Methods: Ber/Ru486@CLPs and Dox@CLGs were prepared by thin-film dispersion and ethanol injection, respectively. To mimic actual TME, the in vitro "condition medium of fibroblasts + MCF-7" cell model and in vivo "4T1/NIH-3T3" co-implantation mice model were established to evaluate the anti-tumor effect of drugs.

Results: The physicochemical properties showed that Dox@CLGs and Ber/Ru486@CLPs were 28 nm and 100 nm in particle size, respectively. In vitro experiments showed that the mixed formulations significantly improved drug uptake and inhibited cell proliferation and migration. The in vivo anti-tumor studies further confirmed the enhanced anti-tumor capabilities of Dox@CLGs + Ber/Ru486@CLPs, including smaller tumor volumes, weak collagen deposition, and low expression levels of α-SMA and CD31 proteins, leading to a superior anti-tumor effect.

Conclusion: In brief, this combination therapy based on Dox@CLGs and Ber/Ru486@CLPs could effectively inhibit tumor development, which provides a promising approach for the treatment of breast cancer.

Keywords: drug delivery, cancer-associated fibroblasts, glucocorticoids, combination therapy

Introduction

Breast cancer is one of the most prevalent malignant tumors worldwide, ranking as the second leading cause of cancer-related fatalities among female subjects.[1,2] Elevated rates of cancer progression, metastasis, and chemotherapy resistance are pivotal factors associated with the diminished survival of breast cancer patients.[3,4] Research has proven that the tumor microenvironment (TME) significantly contributes to these outcomes.[5,6] TME consists of the extracellular matrix (ECM), cytokines and various tumor stromal cells, including fibroblasts, immune cells, inflammatory cells and endothelial cells.[7] The combined strategy of TME-regulating the pro-apoptotic activities has attracted more and more attention in anti-tumor therapy.

Received: 22 January 2024
Accepted: 17 May 2024
Published: 4 June 2024

Cancer-associated fibroblasts (CAFs), as the most abundant stromal cells in TME, are activated from normal fibroblasts,[8] and play an important role in fostering tumor growth.[9,10] Researchers have shown that CAFs could induce epithelial-mesenchymal transitions (EMT) of tumor cells by secreting TGF-β,[11] ultimately leading to tumor metastasis.[12] In addition, CAFs are directly implicated in immunosuppression and drug resistance. They possess the ability to reprogram tumor cell metabolism, and protecting them from apoptosis triggered through treatment.[13–17] Due to the specific distribution and important role of CAFs within tumors, they are increasingly becoming a therapeutic target for the treatment of breast cancer. Berberine (Ber), an isoquinoline quaternary alkaloid extracted from rhizoma coptidis, cortex phellodendri and other medicinal plants, has been proven to possess multiple pharmacological characteristics, including anti-inflammation, antioxidative, anti-diabetic and antitumor activities. Recent research showed that Ber could inhibit CAFs activation,[18,19] collagen deposition, and TGF-β secretion,[20] resulting in the effective suppression of cancer cell metastasis. Hence, the combination of Ber and chemotherapy might be an effective approach to inhibit tumor development.

Furthermore, the majority of breast cancers are hormone-dependent,[21] and hormones could stimulate cancer cell growth by interacting with respective receptors[22] including estrogen receptors, progesterone receptors, glucocorticoid receptors (GR), and androgen receptors.[23,24] Recent research showed that GR was found to be highly expressed in breast cells.[25] Glucocorticoid (GC) interacts with GR to mediate anti-apoptotic actions and induce drug resistance of tumor cells.[26] Hence, hormone-targeting therapy might be an approach for the treatment of breast cancer. Recent research has shown that hormone receptor modulators, such as tamoxifen, anastrozole, exemestane, and letrozole have contributed to the improvement in overall survival rates among breast cancer patients.[27] Mifepristone (Ru486), a GR antagonist and previously used as an abortifacient, has been found to have anti-tumor activity against breast cancer.[28,29] Ru486 could counteract the effects of GC by competitively binding with GR, inhibiting GR dissociation from the heat shock protein complex and post-DNA binding events.[30,31] Hence, Ru486 was considered as a partner with Ber to enhance the inhibition of tumor growth.

Given that chemotherapy combined with TME-regulating therapy have exhibited great potential in efficient treatment of cancers, we design a three-drug combination strategy in which Ber and Ru486 were used to inhibit tumor metastasis caused by the activation of CAFs and GR, respectively, and doxorubicin (Dox) was chosen to induce apoptosis of tumor cells. The synergistic chemotherapy based on combining multiple drugs is a prevalent approach, wherein these drugs are co-administered via the same vehicle.[32] Research has validated that combination therapy could heighten the anti-tumor efficacy, counteract tumor multi-drug resistance, mitigate chemotherapy side effects, and modulate immune function.[33] Nevertheless, the clinical application of chemotherapeutic drugs is limited due to their low solubility, instability in vivo and high toxicity. Nanotechnology offers promise in enhancing chemotherapy effectiveness. Nanoscale carriers, including liposomes, polymer nanoparticles, and nanoparticles, have been developed for drug delivery. Suitable nanocarriers could improve drug solubility, extend circulation duration, achieve sustained drug release, and enhance the safety and bioavailability of drugs.[34,35] Due to abundant CD44 receptor expression of breast cancer cells and CAFs surfaces,[36,37] chondroitin sulfate (CS) was used as a targeting component to improve drug internalization by CS-CD44 receptor-mediated endocytosis.[38] Considering the acidic environment within the tumor, pH-sensitive liposomes (CLPs) co-encapsulated with Ber and Ru486 were prepared. Furthermore, the tight arrangement of tumor cells and the presence of the ECM barrier make it challenging for drug delivery systems. Large-sized nanoparticles (≥ 60 nm) were difficult to deeply penetrate into tumors, leading to insufficient drug concentrations in the core of tumor regions.[39,40] To overcome this, we have prepared small-sized nano-micelles (CLGs) to effectively penetrate the tumor for improved treatment efficacy. CLP standed for chondroitin sulfate (CS)-modified liposomes(LP), and CLG was CS modified nano-micelles comprised of Lipid and Glycocholic acid.

In this study, we synthesized DSPE-PEG-CS polymers and prepared nano-sized delivery systems composed of two types of nanoparticles: CS-modified nano-micelles (Dox@CLGs) and pH-responsive liposomes (Ber/Ru486@CLPs). Dox@CLGs allowed Dox to effectively exert anti-tumor effects, while Ber/Ru486@CLPs were used to regulate TME (Scheme 1), which together exerted synergistic anti-tumor effects. To mimic the TME, a "condition medium of fibroblasts + MCF-7" cell model and a 4T1/NIH-3T3 co-implantation mouse model were established to evaluate anti-tumor efficacy of the mixed formulations in vitro and in vivo, respectively.

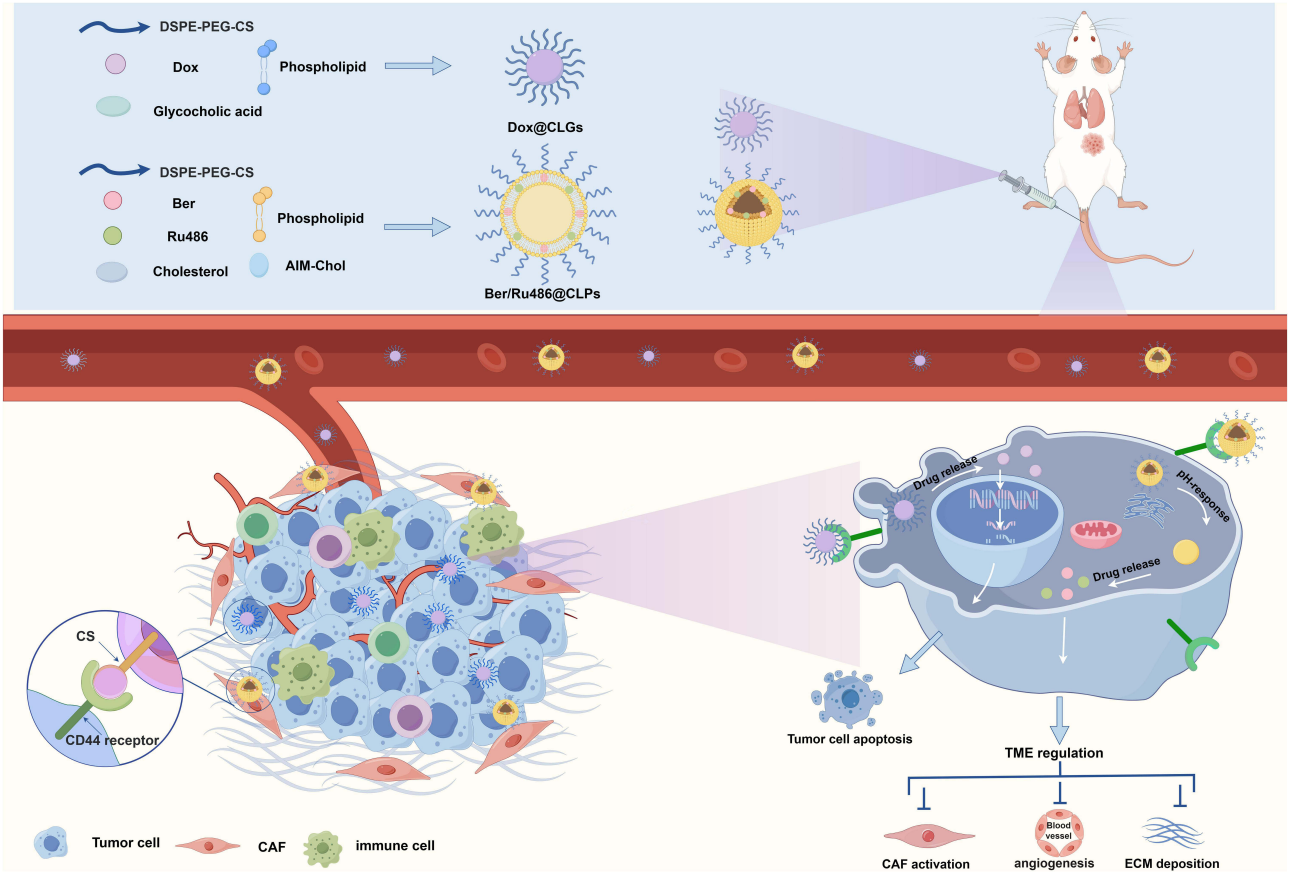

Scheme 1 Schematic diagram of the preparation and antitumor mechanism.

Materials and Methods

Reagents and Materials

Ru486 and glycocholic acid were purchased from Shanghai Macklin Biochemical Co., Ltd. Doxorubicin (Dox), DMEM and RPMI-1640 medium were acquired from Dalian Meilun Biology Technology Co., Ltd. Fetal bovine serum (FBS) was procured from Excell Biological Technology Co., Ltd. Ber was obtained from Beijing InnoChem Science & Technology Co., Ltd. α-SMA antibody (cat. AF1032) was acquired from Affinity Biosciences Pty Ltd. All of the schematic diagrams, including Scheme 1 and the schemes in other figures, had been created with FigDraw.com with permission.

Cell Lines and Animals

The human breast carcinoma cell lines MCF-7, human fibroblasts cell lines MRC-5, mouse breast cancer cell line 4T1, and mouse fibroblasts cell lines NIH-3T3 were purchased from the China Center for Type Culture Collection. MCF-7 and NIH-3T3 cell lines were maintained in DMEM medium plus 10% FBS. The 4T1 cell line was cultivated in RPMI-1640 medium supplemented with 10% FBS. The MRC-5 cell line was sustained in Minimum Essential Medium and also supplemented with 10% FBS. The cell lines were cultured and maintained in a humidified incubator with 5% CO_2 at 37°C. The condition medium (CM) of MRC-5 cells was obtained according to our previous method. In the mixed cell culture model, a ratio of 4T1 cells to NIH-3T3 cells at 5:1 was employed.

Female Balb/c mice (5–7 weeks) were purchased from Jinan Pengyue Experimental Animal Breeding Co., Ltd. All animal experiments were approved by the Animal Ethics Committee of Shandong Second Medical University, and the care and handling procedures strictly complied with “Guide for the Care and Use of Laboratory Animals” of China (D.N. 55, 2001).

Preparation and Characterization of Dox@CLGs and Ber/Ru486@CLPs

The Ber/Ru486@CLPs were prepared using the ethanol injection method. AIM-Chol was synthesized as previously described.[41] A solution comprising 120 mg of phospholipid (PL), 30 mg of cholesterol, 10 mg of AIM-Chol, and 4 mg of chondroitin sulfate-modified conjugates (DSPE-PEG-CS) were dissolved in ethanol, followed by the addition of Ber and Ru486 at varying concentrations (4 mg, 6 mg, and 12 mg each), respectively. Ethanol was subsequently removed through rotary evaporation at 60°C. The resulting suspension was sonicated in an ultrasonic cell crusher (VCX750) for 15 minutes in an ice water bath and then extruded three times through a 220 nm polycarbonate membrane to yield the Ber/Ru486@CLPs liposomes.

The prepared route for the nano-micelles Dox@CLGs was outlined as follows. Initially, 110 mg of glycocholic acid was dissolved in a phosphate buffer saline (PBS) solution with the pH adjusted to approximately 5.5. Subsequently, 90 mg of PL, 5.5 mg of Dox, and 4 mg of DSPE-PEG-CS were dissolved in an ethanol solution. The ethanol solution containing the drugs was slowly introduced into the glycinylcholic acid solution. Ethanol was eliminated through rotary evaporation at 55°C. The same procedure was applied for sonication and extrusion through a 220 nm polycarbonate membrane. The preparation of Dox@LGs and Ber/Ru486@LPs were similar to that of Dox@CLGs and Ber/Ru486@CLPs. In parallel, DiR@LGs and DiR@CLGs were prepared by substituting Dox with DiR with a similar preparation process.

Dynamic light scattering (DLS) and electrophoretic light scattering techniques were employed to assess size distribution and zeta potential. Specifically, 100 μL of each nanoparticle was suspended in 1 mL of PBS and analyzed using a Malvern Zetasizer ZS 90. The morphology of Dox@CLGs and Ber/Ru486@CLPs were examined via transmission electron microscope (TEM, Hitachi HT7700). Drug loading (DL) and encapsulation efficiency (EE) in nanoparticles was determined through UV spectrophotometry.

Cellular Uptake

CM/MCF-7 cells were seeded in 24-well plates (1×10^5 cells/well) and cultured overnight. The medium was removed and Dox, Dox@LGs, and Dox@CLGs (Dox: 10 μg/mL) were then added to each well and incubated for 3 h. The red fluorescence of Dox was employed to assess the cellular uptake of nano-micelles within the cells. Coumarin 6 (C6), a hydrophobic fluorescent dye, is commonly used to facilitate the traceability of nano drug delivery systems in vitro.[42,43] In this study, C6 was utilized to monitor the distribution of liposomes. Likewise, an equivalent solution of C6, C6@LPs, and C6@CLPs (C6: 10 μg/mL) was incubated for 3 h. Subsequently, the cells were washed with PBS and the fluorescence intensity was measured using confocal laser scanning microscopy (CLSM) and flow cytometry.

Cell Viability Assay

MCF-7 cells were cultured with the condition medium (CM) of MRC-5 cells to build a "CM/MCF-7" cell research model to mimic TME. Cell viability was assessed against CM/MCF-7 cells at a drug concentration from 0.01 to 5 μg/mL using the MTT assay. Briefly, the cells were seeded at a density of 5×10^3 cells per well in 96-well plates, with each well containing 100 μL of complete medium. After cell attachment, they were exposed to various drug solutions for 48 h. MTT solution (5 mg/mL) was added to each well for 4 h incubation at 37°C. Then MTT solution was removed from the wells, and DMSO (150 μL/well) was added to dissolve the formazan crystals within the cells. Absorbance readings were obtained at 490 nm using a BioTek EXL800 microplate reader. Cell viability was quantified as the percentage of absorbance in the drug-treated group relative to the vehicle-treated group.

Wound Healing Assay

CM/MCF-7 cells were cultured in 6-well plates (2×10^5 cells/well) and allowed to adhere to the culture plate. A scratch was made across the cell monolayer in each well using a 200 μL sterile pipette tip, and the detached cells were subsequently removed by washing with PBS. The cells were then cultured in different drug formulations (Ber + Ru486, Ber/Ru486@CLPs, Dox, Dox@CLGs, Dox + Ber + Ru486 and Dox@CLGs + Ber/Ru486@CLP). Images of the CM/MCF-7 cells were captured at 0 h and 24 h later. Image J software was used to measure the scratch area and the rate of wound closure was calculated.

Hemolytic Study of Dox@CLGs and Ber/Ru486@CLPs

Blood was collected from Balb/c mice into heparinized blood collection tubes. Next, 2 mL of the blood was washed by mixing with PBS, followed by centrifugation at 10,000 g for 10 min. The obtained cells were resuspended in 10 mL of PBS. Then, 0.2 mL of the cell suspension was mixed with 0.8 mL of different nanoparticle concentrations (0.5, 1, 2, 4, 5 mg/mL). After incubating overnight, the supernatant was collected by centrifugation, and its absorbance was measured to calculate the hemolysis ratio. The treatment of Triton X-100 and PBS served as positive and negative controls, respectively.

In vivo Imaging

To investigate the in vivo drug distribution, a suspension of 1×10^6 4T1 cells was subcutaneously injected into the right flanks of the Balb/c mice. Additionally, 1×10^6 4T1 cells were injected via the tail vein one week after 4T1 cell implantation. 0.2 mL of free DiR, DiR@LGs, and DiR@CLGs (4 mg/kg) were administered separately to the tumor-bearing mice via the tail vein. The IVIS imaging system was employed to assess the in vivo biodistribution at various time points (0, 2, 8, 12, 24, 36, and 48 h). After 48 h of DiR preparation injection, tumor-bearing mice were anaesthetized using a mixture of ketamine (60 mg/kg) and xylazine (5 mg/kg). Subsequently, mice were humanely euthanized to harvest tumors and organs, and their fluorescence intensities were measured.

Antitumor Efficacy in Subcutaneous Tumor Model

To establish TME-like subcutaneous tumor mice models, a suspension of 1×10^6 4T1/NIH-3T3 cells were subcutaneously injected into the right flanks of the Balb/c mice. Once the tumors reached a volume of approximately 80 mm^3, the mice were randomly divided into 7 groups (5 mice per group), including saline, Ber + Ru486, Ber/Ru486@CLPs, Dox, Dox@CLGs, Dox + Ber + Ru486 and Dox@CLGs + Ber/Ru486@CLPs (Dox: 3 mg/kg; Ber: 3 mg/kg). Injections were administered every two days while tumor volume and body weight were measured. After two weeks of treatment, the mice were anaesthetized using ketamine and xylazine. Subsequently, the animals were humanely euthanized, and their organs and tumors were collected for subsequent H&E staining, immunohistochemical (IHC) analysis and flow cytometry.

Statistical Analysis

All data were presented as means ± standard deviation (SD). Different groups were compared by one-way analysis of variance (ANOVA) or two-way ANOVA. Graphpad Prism 9.0.0 was used for statistical analysis. All experiments were performed with at least three replicates. $P < 0.05$ was considered statistically significant.

Results and Discussion

Characterizations of Dox@CLGs and Ber/Ru486@CLPs

Dox@CLGs and Ber/Ru486@CLPs were prepared to inhibit tumor proliferation. Table 1 showed that the DL of Dox@CLGs was 4.91%, and Ber/Ru486@CLPs possessed high drug loading for Ber (6.07%) and Ru486 (4.19%). In Figure 1A and B, both formulations exhibited a similar spherical morphology. Notably, Dox@CLGs had a smaller size (28.77 nm) in comparison with Ber/Ru486@CLPs (102.37 nm). Considering high density and limited interstitial spaces of tumor tissues,[44,45] smaller nanoparticles could penetrate tumor tissues effectively, potentially enhancing anti-tumor effects. The zeta potentials were −22.6 mV and −15.63 mV for Dox@CLGs and Ber/Ru486@CLPs, respectively. These negative zeta potential values are pivotal to prevent non-specific cellular uptake and improve delivery efficiency. Furthermore, the particle sizes and polydispersity index (PDI) of Ber/Ru486@CLPs and Dox@CLGs were measured in DMEM medium for 14 days. The results in Figure 1C and D showed that no significant differences were observed in the two formulations, suggesting that the two nano-sized carriers had good stability under physiological conditions. The hemolysis rates of Dox@CLGs and Ber/Ru486@CLPs were found to be only 0.16% and 0.32%, respectively (Figure 1E), indicating that they did not induce hemolysis at various concentrations and demonstrating good blood compatibility.

Table 1 Characterizations of Dox@CLGs and Different Ber/Ru486@CLPs Formulations

	DLS (nm)	PDI	Potential (mV)	EE (%)	DL (%)
Dox@CLGs	28.77±0.19	0.17±0.01	−22.6±2.02	95.07±2.39	4.91±0.12
CLP: B/R (41.0:1)	98.57±0.86	0.17±0.01	−12.63±1.30	91.72±0.02	2.18±0.01 (B)
				67.25±0.47	1.60±0.01 (R)
CLP: B/R (27.3:1)	103.73±1.30	0.18±0.01	−13.37±0.64	95.54±2.14	3.33±0.07 (B)
				64.52±1.91	2.25±0.07 (R)
CLP: B/R (13.7:1)	102.37±1.62	0.18±0.01	−15.63±0.32	93.10±1.10	6.07±0.07 (B)
				64.18±2.58	4.19±0.17 (R)

Abbreviations: B, Ber; R, Ru486.

Cellular Uptake

Figure 2A displayed fluorescence images of CM/MCF-7 cells after 3 h of incubation with free Dox, Dox@LGs, and Dox@CLGs. Notably, more red fluorescent signals were observed in Dox@CLGs than other groups. CD44 is known to be highly expressed on the surface of tumor cells and CAFs, and it has a high affinity for CS.[46,47] CS-modified carriers could bind to the CD44 receptors on the surface of MCF-7, leading to massive uptake of drugs. Furthermore, Figure 2B

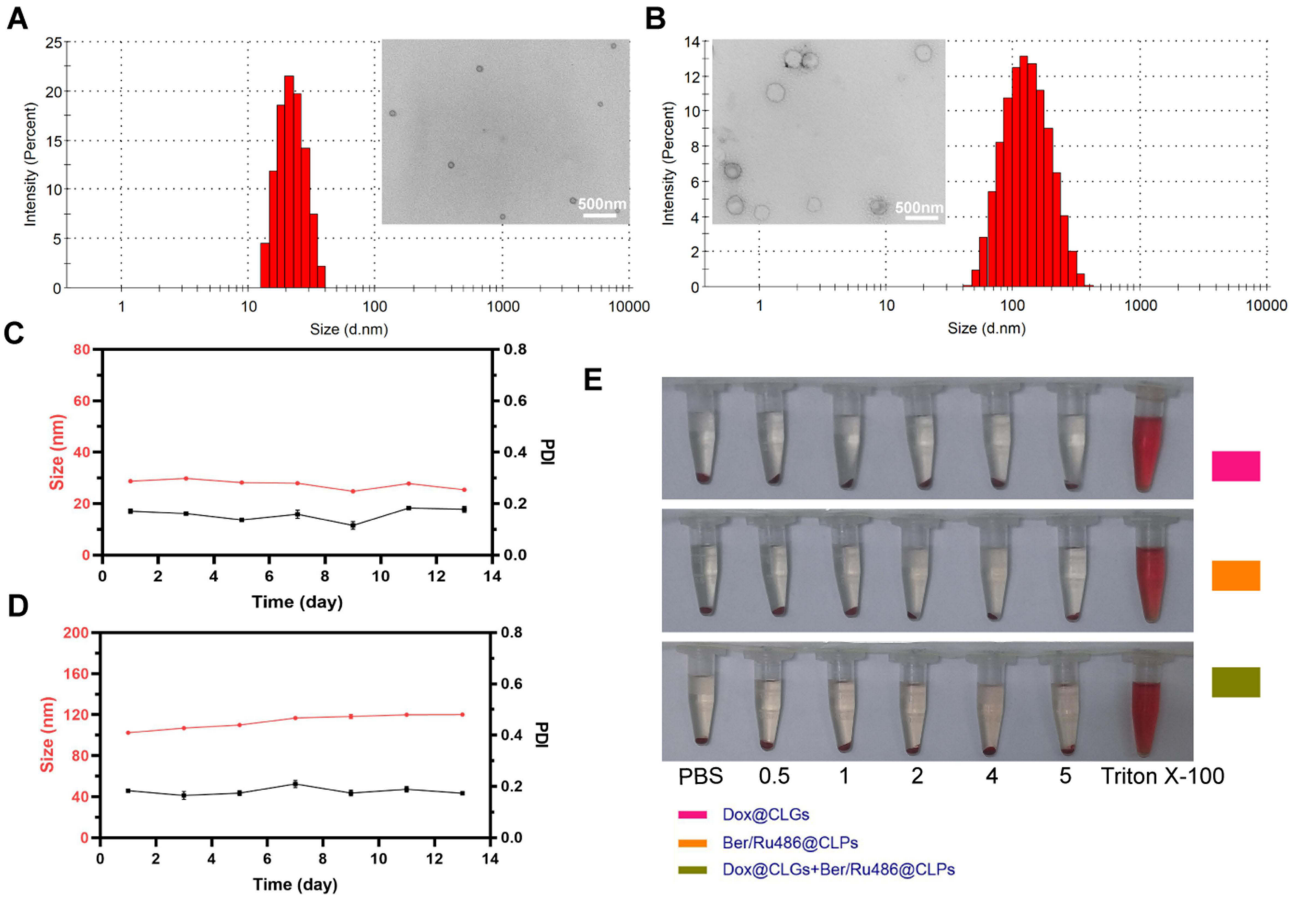

Figure 1 Characterizations of Dox@CLGs and Ber/Ru486@CLPs.
Notes: (**A**) The TEM images of the Dox@CLGs and (**B**) Ber/Ru486@CLPs. (**C**) Changes of hydrodynamic diameter and PDI of Dox@CLGs and (**D**) Ber/Ru486@CLPs for 14 days. (**E**) Hemolytic study of Dox@CLGs and Ber/Ru486@CLPs for different concentrations (mg/mL).

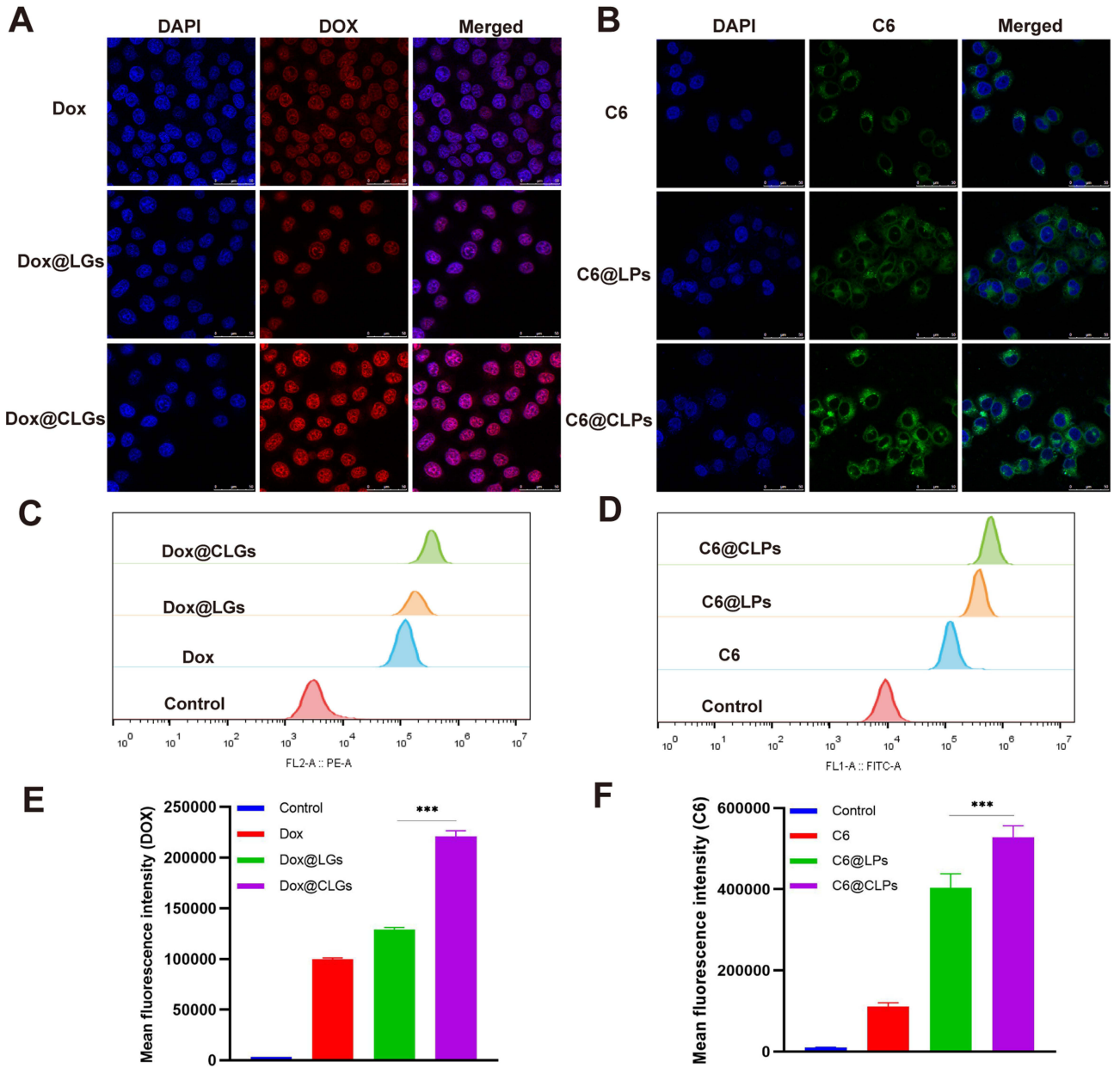

Figure 2 Cellular uptake.
Notes: (**A**) CLSM images of Dox@CLGs and (**B**) Ber/Ru486@CLPs uptake by CM/MCF-7 cells. Blue, red, and green represent DAPI, Dox, and C6 fluorescence, respectively. (**C**) Flow cytometry of Dox@CLGs and (**D**) Ber/Ru486@CLPs uptake. (**E** and **F**) The quantified mean fluorescence intensity in different groups. ***$p < 0.001$.

showed the cellular uptake of liposomes by CM/MCF-7 cells. The groups treated with free C6 and C6@LPs displayed weak green fluorescence signals, while stronger green fluorescence was detected in the mixed cells in the C6@CLPs group, indicating that CS-modified liposomes promoted drug uptake. Similar results were observed with flow cytometry (Figure 2C and D) and their quantitative results (Figure 2E and F). These results suggested that both CLGs and CLPs could target MCF-7 via CS-CD44-mediated endocytosis, resulting in enhanced drug internalization.

In vitro Cytotoxicity and Cell Migration Analysis

The cytotoxicity of different formulations against CM/MCF-7 cells was measured by MTT assay Figure 3A). As shown in Figure 3B, an obvious concentration-dependent inhibitory effect was observed in all drug-treated groups. After 48 h of co-incubation, the IC50 value of free Dox was 0.659 μg/mL and 0.472 μg/mL for Dox@CLGs, indicating stronger anti-

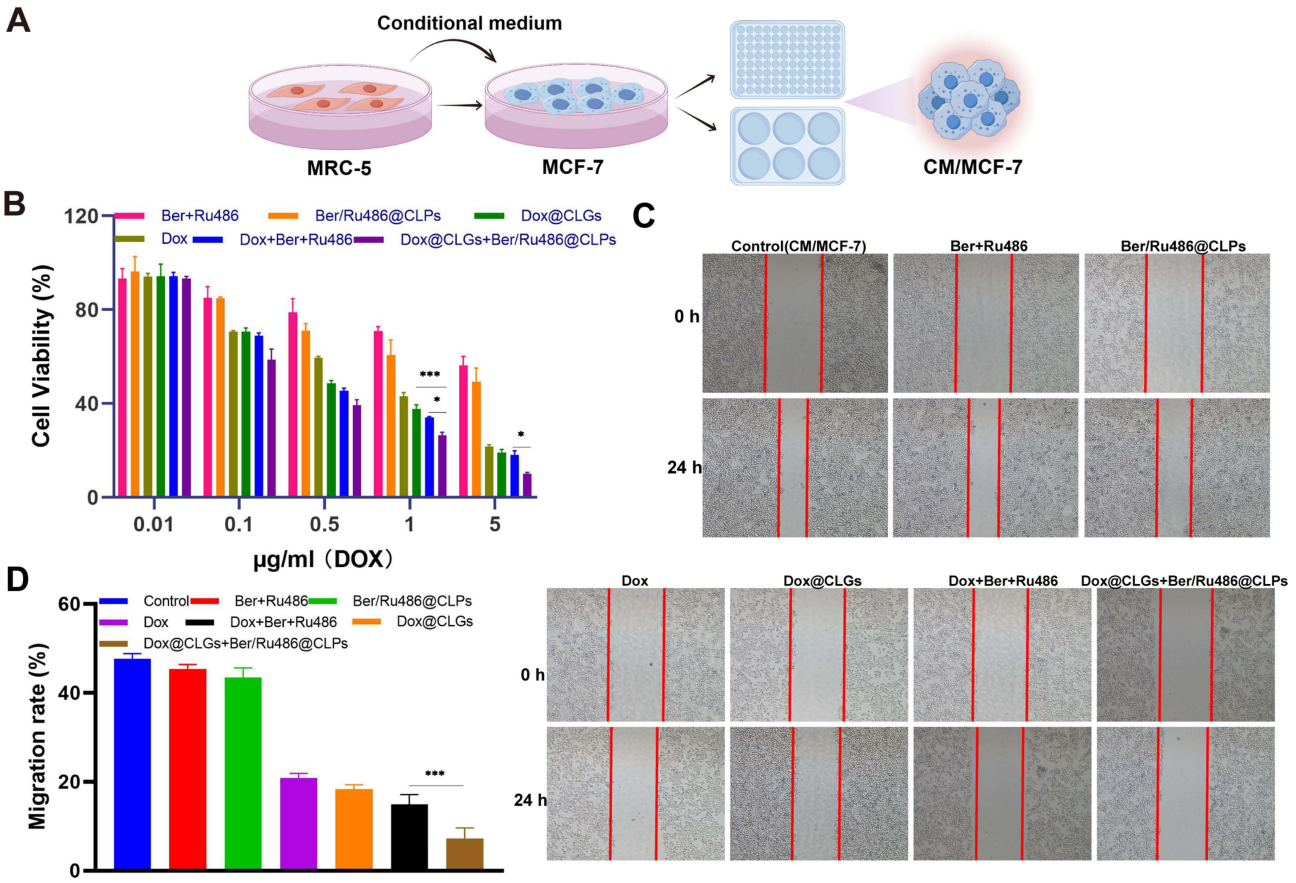

Figure 3 In vitro experiments of Dox@CLGs and Ber/Ru486@CLPs.
Notes: (**A**) The pattern diagram of CM/MCF-7 cells. (**B**) Cell viability of CM/MCF-7 cells after different formulations treatment at 48 h. (**C** and **D**) Wound healing assay for CM/MCF-7. ***p < 0.001, *p < 0.05.

proliferation effect. Interestingly, compared with Dox@CLGs and Ber/Ru486@CLPs, the cell survival rate in Dox@CLGs + Ber/Ru486@CLPs was lower. This result might be due to the fact that Ber/Ru486@CLPs could improve the sensitivity of Dox,[48] leading to stronger anti-proliferation effects. These results suggested that the combination of Dox@CLGs and Ber/Ru486@CLPs had potent cytotoxicity against cancer cells and was expected to block CAF-induced tumor growth.

Cell migration was assessed by the wound healing assay. The scratch areas were shown in Figure 3C and D. The migration rate was 45.5% and 43.3% in Ber + Ru486 and Ber/Ru486@CLPs. There is an obviously deceased in the presence of Dox, suggesting that Ber + Ru486 alone could not effectively inhibit tumor migration. Interestingly, the cells treated with Dox@CLGs + Ber/Ru486@CLPs showed a lower migratory rate than Dox + Ber + Ru486 and Dox@CLGs. This result might be due to two reasons: (1) nano-sized vehicles improved drug-reduced anti-migration effect; (2) the presence of Ber and Ru486 improved the sensitivity of Dox against CM/MCF-7 cells.

In vivo Biodistribution

The biodistribution of Dox@CLGs was investigated in 4T1 tumor-bearing mice using DiR-labeled nanoparticles. As shown in Figure 4A, the fluorescence rapidly disappeared in the free DiR group. However, in the nano-micelles groups, the fluorescent signals were maintained for a longer time in mice, suggesting that CLGs improved the long-circulating time of drugs. After 48 h, the DiR@CLGs group showed higher fluorescence intensity than DiR@LGs, indicating that CS modification promoted drug accumulation in tumor regions. The fluorescence imaging of main organs and tumor was presented in Figure 4B. The results showed that there were only weak DiR signals in free DiR at the tumor tissue, while DiR@CLGs showed stronger fluorescence (Figure 4B and C). This possible explanation was that DiR@CLGs could

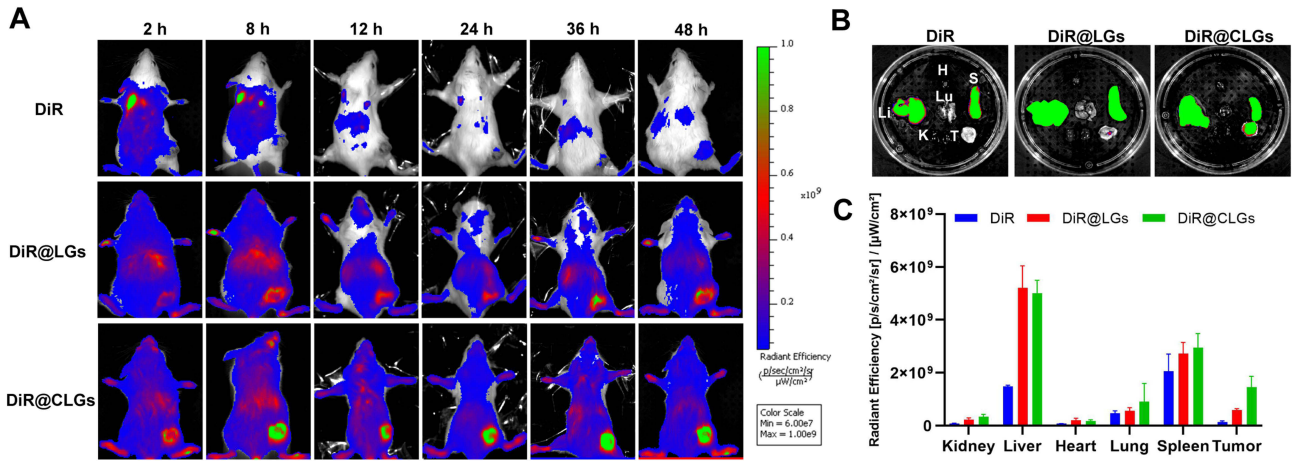

Figure 4 In vivo imaging.
Notes: (**A**) Biodistribution analysis of 4T1 tumor-bearing mice after intravenous injection of DiR, DiR@LGs, or DiR@CLGs at different time points. (**B**) Fluorescence images of isolated organs and tumor tissues. (**C**) Quantitative analysis.

accumulate in the tumor site through EPR- and CS-CD44 receptor-mediated delivery,[49] leading to high drug distribution in tumor regions. Considering that lack of tumor-targeting properties was the main cause of systemic effects of traditional drug formulations, CLGs might be a potential carrier for drug delivery.

Anti-Tumor Efficacy in Subcutaneous Tumor Model

TME plays an important role in breast cancer development.[50,51] The in vivo antitumor efficacy of different drug formulations was assessed in the 4T1/NIH-3T3 subcutaneous tumor model (Figure 5A). Compared with the saline group, no significant weight loss was observed in three nano-sized formulations during the treatment period (Figure 5B), indicating that CLGs and CLPs were safe drug delivery systems. As shown in Figure 5C, Dox@CLGs showed smaller tumor volumes than the free Dox group, suggesting that CLGs could promote Dox-induced anti-tumor effects. Moreover, Dox@CLGs + Ber/Ru486@CLPs exhibited an average tumor volume less than half of the Dox@CLGs or Ber/Ru486@CLPs group, indicating its robust synergistic anti-tumor efficacy. This result was also confirmed by the tumor morphology and inhibition rates in Figure 5D and E, in which Dox@CLGs + Ber/Ru486@CLPs exhibited smaller tumor sizes and higher inhibitory rates than other groups. Histological and immunohistochemical analyses were used to further evaluate the antitumor activity. H&E staining showed that obvious cell damage was observed in the Dox@CLGs + Ber/Ru486@CLPs group, with large-scale cell apoptosis and unclear cell contours (Figure 5F), indicating that the combination therapy based on nano-sized carriers showed significant pro-apoptotic effects. In TME, CAFs facilitate ECM deposition by secreting a large amount of collagen and fibronectin which creates a barrier around tumor cells that prevents chemotherapy drugs from entering.[52,53] To examine extracellular matrix deposition, Masson staining was performed. As shown in Figure 5G, amounts of blue signal appeared in the control group while there are nearly no signal in Dox + Ber + Ru486 and Dox@CLGs + Ber/Ru486@CLPs groups, suggesting that the three-drug synergistic therapy effectively inhibited ECM deposition. Moreover, α-SMA, a marker for CAFs,[54,55] was stained brown in Figure 5H. Compared with Dox@CLGs, Dox@CLGs + Ber/Ru486@CLPs had fewer brown areas, indicating a stronger anti-CAFs effect. These results suggested that the combination of Dox@CLGs and Ber/Ru486@CLPs exerted anti-tumor effects through inhibition of CAFs and reduction of ECM deposition. Additionally, the expression of CD31 (an angiogenesis marker[56]) was significantly reduced in Dox@CLGs + Ber/Ru486@CLPs group in comparison with the other groups (Figure 5I), indicating that Dox@CLGs + Ber/Ru486@CLPs could effectively inhibit tumor angiogenesis. These results showed that Dox@CLGs + Ber/Ru486@CLPs exhibited superior synergistic anti-tumor effects by pro-apoptotic and TME-regulating activities.

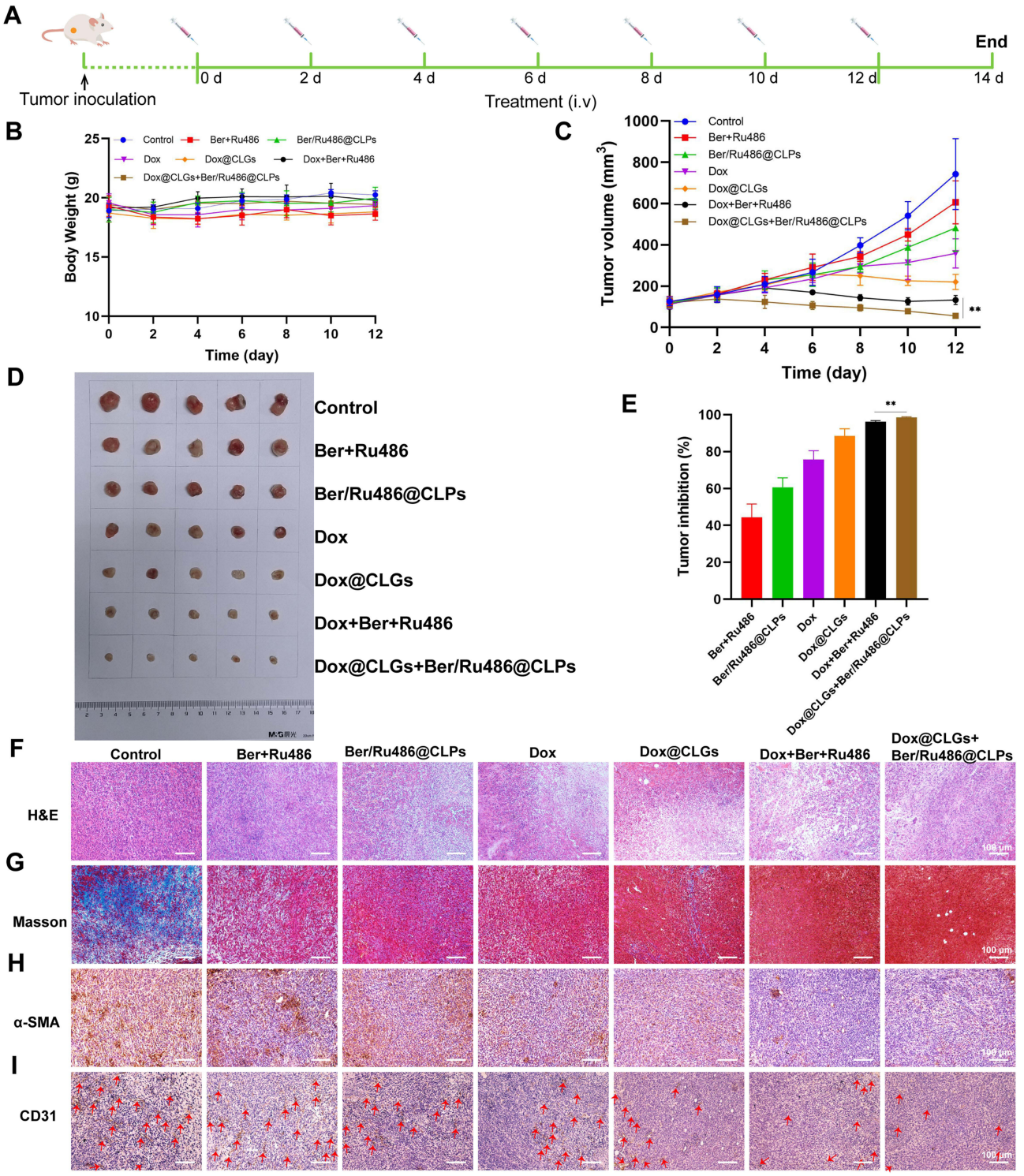

Figure 5 Subcutaneous antitumor effect in vivo.

Notes: (**A**) Schedule for subcutaneous 4T1/NIH-3T3 tumor model establishment and treatment. (**B**) Body weight changes during the treatment. (**C**) tumor growth curves of tumor-bearing mice. (**D**) The anatomy of the tumor after different treatments. (**E**) Tumor inhibition. Histological and immunohistochemical analysis of (**F**) H&E, (**G**) Masson, (**H**) α-SMA, and (**I**) CD31 assays for tumor tissue. **p < 0.01.

Biosafety

To assess biosafety, possible adverse effects of Dox@CLGs and Ber/Ru486@CLPs were examined after 14 days of treatment. As illustrated in Figure 6A, H&E staining revealed no substantial change in the main organs (heart, liver,

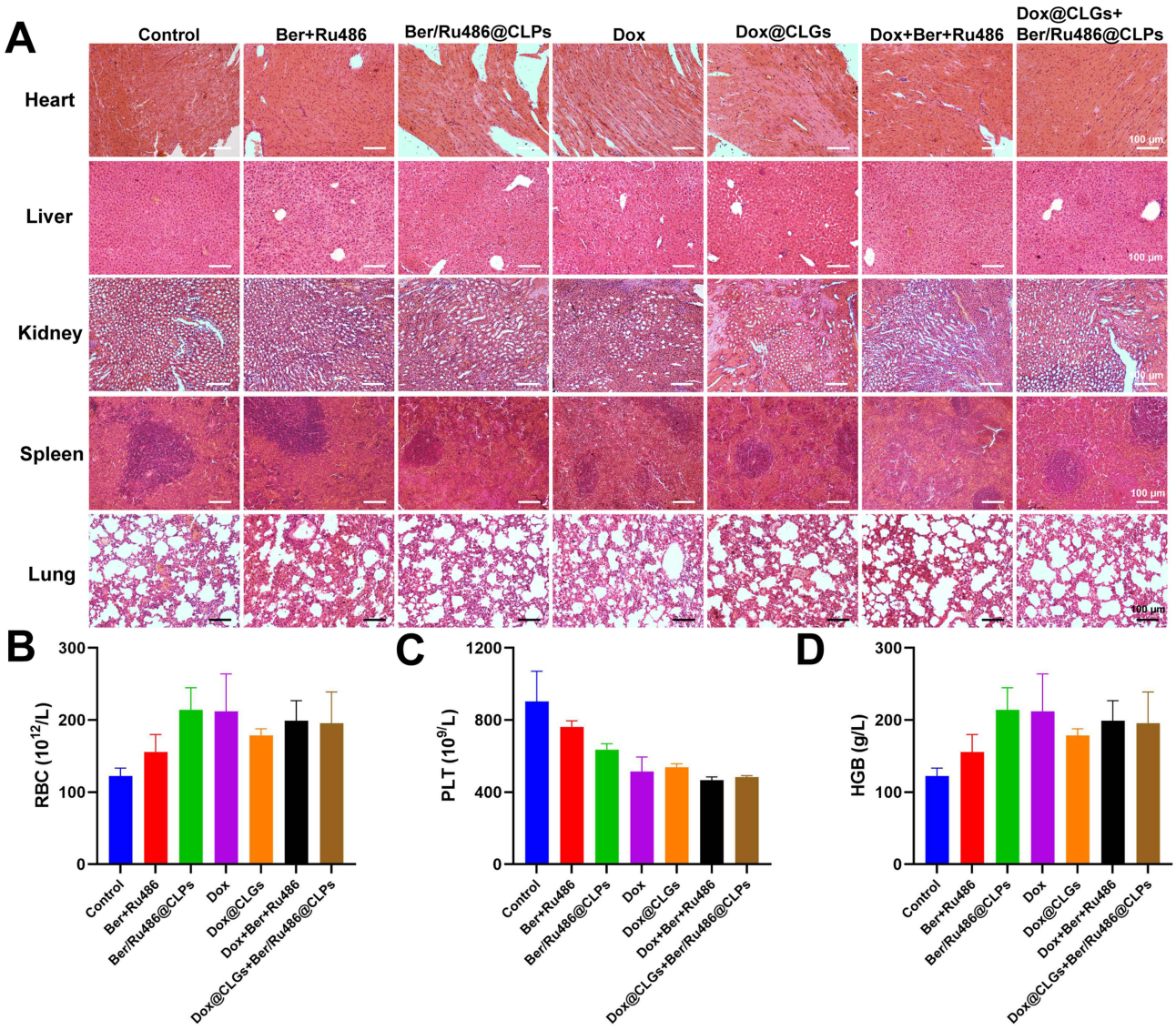

Figure 6 The safety profile of Dox@CLGs and Ber/Ru486@CLPs.
Notes: (**A**) H&E assay of the major organs (heart, liver, kidney, spleen, and lung). Blood cells levels of (**B**) RBC, (**C**) PLT, and (**D**) HGB.

spleen, lung, and kidney) in nano-sized drug groups This indicated that Dox@CLGs and Ber/Ru486@CLPs exhibited sufficient biosafety. Additionally, routine blood tests were performed on normal Balb/c mice. The indexes of red blood cells (RBC), platelets (PLT), and hemoglobin (HGB) (Figure 6B–D) showed no significant difference among the drug-treated mice. These results confirmed the excellent biocompatibility of Dox@CLGs and Ber/Ru486@CLPs, suggesting that CLGs and CLPs were promising and safe formulations for antitumor therapy.

Conclusion

In summary, we developed a novel anti-tumor strategy by combining modulation of TME and chemotherapy based on mixed nano-delivery systems. Notably, Dox@CLGs showed excellent cellular uptake and tumor-targeting delivery properties. Dox@CLGs + Ber/Ru486@CLPs improved cytotoxicity and anti-migration effect of drugs in vitro. This nano-formulation has the potential to overcome the limitations of traditional nano-systems, including non-specific targeting, low permeability, and immune tolerance. They exhibit superior physicochemical characteristics and biological properties when compared to other carrier systems. Moreover, the in vivo experiments indicated that Dox@CLGs + Ber/Ru486@CLPs exhibited smaller tumor volume, less ECM deposition and tumor angiogenesis than other groups. The

combination of Dox@CLGs and Ber/Ru486@CLPs possesses superior anti-tumor effects, which provides a promising approach for breast cancer treatment. The nano-sized formulations composed of CLP and CLG provide an effective anti-cancer approach, and the formulation optimization and in-depth analysis of anti-tumor mechanisms are necessary for clinical application.

Author Contributions

All authors made a significant contribution to the work reported, whether that is in the conception, study design, execution, acquisition of data, analysis and interpretation, or in all these areas; took part in drafting, revising or critically reviewing the article; gave final approval of the version to be published; have agreed on the journal to which the article has been submitted; and agree to be accountable for all aspects of the work.

Funding

This work was supported by the National natural Science Foundation of China (No. 81803464), the Medical & Health Development Plan Project of Shandong Province (No. 202213020516), the Science and Technology Development Program in Weifang (No. 2021GX053, 2022ZJ1064) and the Scientific Research Project of Weifang University of Science and Technology (No. 2022KJ02).

Disclosure

The authors report no conflicts of interest in this work.

References

1. Koual M, Tomkiewicz C, Cano-Sancho G, Antignac J-P, Bats A-S, Coumoul X. Environmental chemicals, breast cancer progression and drug resistance. *Environ Health*. 2020;19(1). doi:10.1186/s12940-020-00670-2
2. Jokar N, Velikyan I, Ahmadzadehfar H, et al. Theranostic approach in breast cancer. *Clin Nucl Med*. 2021;46(8):e410–e420. doi:10.1097/RLU.0000000000003678
3. Scimeca M, Urbano N, Bonfiglio R, et al. Novel insights into breast cancer progression and metastasis: a multidisciplinary opportunity to transition from biology to clinical oncology. *Bioch et Bio Acta*. 2019;1872(1):138–148. doi:10.1016/j.bbcan.2019.07.002
4. Gote V, Nookala AR, Bolla PK, Pal D. Drug resistance in metastatic breast cancer: tumor targeted nanomedicine to the rescue. *Int J Mol Sci*. 2021;22(9):4673. doi:10.3390/ijms22094673
5. Mehraj U, Dar AH, Wani NA, Mir MA. Tumor microenvironment promotes breast cancer chemoresistance. *Cancer Chemother Pharmacol*. 2021;87(2):147–158. doi:10.1007/s00280-020-04222-w
6. Xiao Y, Yu D. Tumor microenvironment as a therapeutic target in cancer. *Pharmacol Ther*. 2021;2021:221.
7. Lüönd F, Tiede S, Christofori G. Breast cancer as an example of tumour heterogeneity and tumour cell plasticity during malignant progression. *Br J Cancer*. 2021;125(2):164–175. doi:10.1038/s41416-021-01328-7
8. Qiao A, Gu F, Guo X, Zhang X, Fu L. Breast cancer-associated fibroblasts: their roles in tumor initiation, progression and clinical applications. *Front Med*. 2016;10(1):33–40. doi:10.1007/s11684-016-0431-5
9. Hu D, Li Z, Zheng B, et al. Cancer-associated fibroblasts in breast cancer: challenges and opportunities. *Cancer Commun*. 2022;42(5):401–434. doi:10.1002/cac2.12291
10. Piersma B, Hayward M-K, Weaver VM. Fibrosis and cancer: a strained relationship. *Bioch et Bio Acta*. 2020;1873(2):188356. doi:10.1016/j.bbcan.2020.188356
11. Wu F, Yang J, Liu J, et al. Signaling pathways in cancer-associated fibroblasts and targeted therapy for cancer. *Signal Transduct Target Ther*. 2021;6(1):218. doi:10.1038/s41392-021-00641-0
12. Hao Y, Baker D, Ten Dijke P. TGF-beta-mediated epithelial-mesenchymal transition and cancer metastasis. *Int J Mol Sci*. 2019;20(11):2767. doi:10.3390/ijms20112767
13. Mhaidly R, Mechta-Grigoriou F. Role of cancer-associated fibroblast subpopulations in immune infiltration, as a new means of treatment in cancer. *Immunol Rev*. 2021;302(1):259–272. doi:10.1111/imr.12978
14. Huang H, Wang Z, Zhang Y, et al. Mesothelial cell-derived antigen-presenting cancer-associated fibroblasts induce expansion of regulatory T cells in pancreatic cancer. *Cancer Cell*. 2022;40(6):656–673 e657. doi:10.1016/j.ccell.2022.04.011
15. Caligiuri G, Tuveson DA. Activated fibroblasts in cancer: perspectives and challenges. *Cancer Cell*. 2023;41(3):434–449. doi:10.1016/j.ccell.2023.02.015
16. Mhaidly R, Mechta-Grigoriou F. Fibroblast heterogeneity in tumor micro-environment: role in immunosuppression and new therapies. *Semin Immunol*. 2020;48:101417. doi:10.1016/j.smim.2020.101417
17. Costa A, Kieffer Y, Scholer-Dahirel A, et al. Fibroblast heterogeneity and immunosuppressive environment in human breast cancer. *Cancer Cell*. 2018;33(3):463–479 e410. doi:10.1016/j.ccell.2018.01.011
18. Tsang CM, Cheung YC, Lui VW, et al. Berberine suppresses tumorigenicity and growth of nasopharyngeal carcinoma cells by inhibiting STAT3 activation induced by tumor associated fibroblasts. *BMC Cancer*. 2013;13:619. doi:10.1186/1471-2407-13-619
19. Wang Y, Liao J, Luo Y, et al. Berberine alleviates doxorubicin-induced myocardial injury and fibrosis by eliminating oxidative stress and mitochondrial damage via promoting Nrf-2 pathway activation. *Int J Mol Sci*. 2023;24(4):1.

20. Ai F, Chen M, Yu B, et al. Berberine regulates proliferation, collagen synthesis and cytokine secretion of cardiac fibroblasts via AMPK-mTOR-p70S6K signaling pathway. *Int J Clin Exp Pathol*. 2015;8(10):12509–12516.
21. Gompel A. Hormone and breast cancer. *Presse Med*. 2019;48(10):1085–1091. doi:10.1016/j.lpm.2019.09.021
22. Boszkiewicz K, Sawicka E, Piwowar A. The impact of xenoestrogens on effectiveness of treatment for hormone-dependent breast cancer - current state of knowledge and perspectives for research. *Ann Agric Environ Med*. 2020;27(4):526–534. doi:10.26444/aaem/124165
23. Fabris VT, Spring L, Helguero LA. Editorial: steroid hormone receptors and cell cycle in breast cancer. *Front Endocrinol*. 2023;14:1196523. doi:10.3389/fendo.2023.1196523
24. Wang X, Yang D. The regulation of RNA metabolism in hormone signaling and breast cancer. *Mol Cell Endocrinol*. 2021;529:111221. doi:10.1016/j.mce.2021.111221
25. Vilasco M, Communal L, Mourra N, Courtin A, Forgez P, Gompel A. Glucocorticoid receptor and breast cancer. *Breast Cancer Res Treat*. 2011;130(1):1–10. doi:10.1007/s10549-011-1689-6
26. Capunzo M, Caraglia M, Cianciola E, et al. Potential mechanisms by which glucocorticoids induce breast carcinogenesis through Nrf2 inhibition. *Front Biosci*. 2022;27(7):1.
27. Barchiesi G, Mazzotta M, Krasniqi E, et al. Neoadjuvant Endocrine Therapy In Breast Cancer: Current Knowledge And Future Perspectives. *Int J Mol Sci*. 2020;21(10):3528. doi:10.3390/ijms21103528
28. Liu R, Shi P, Nie Z, et al. Mifepristone suppresses basal triple-negative breast cancer stem cells by down-regulating KLF5 expression. *Theranostics*. 2016;6(4):533–544. doi:10.7150/thno.14315
29. Didonato JA, Saatcioglu F, Karin M. Molecular mechanisms of immunosuppression and anti-inflammatory activities by glucocorticoids. *Am J Respir Crit Care Med*. 1996;154(2):S11–15. doi:10.1164/ajrccm/154.2_Pt_2.S11
30. Bamberger CM, Chrousos GP. The glucocorticoid receptor and RU 486 in man. *Ann N Y Acad Sci*. 1995;761:296–310. doi:10.1111/j.1749-6632.1995.tb31385.x
31. Agarwai MK. The antiglucocorticoid action of mifepristone. *Pharmacol Ther*. 1996;70(3):183–213. doi:10.1016/0163-7258(96)00016-2
32. Li B, Shao H, Gao L, Li H, Sheng H, Zhu L. Nano-drug co-delivery system of natural active ingredients and chemotherapy drugs for cancer treatment: a review. *Drug Delivery*. 2022;29(1):2130–2161. doi:10.1080/10717544.2022.2094498
33. Zhang Y, Lou Y, Wang J, Yu C, Shen W. Research status and molecular mechanism of the traditional Chinese medicine and antitumor therapy combined strategy based on tumor microenvironment. *Front Immunol*. 2020;11:609705. doi:10.3389/fimmu.2020.609705
34. Gomes ER, Franco MS. Combining nanocarrier-assisted delivery of molecules and radiotherapy. *Pharmaceutics*. 2022;14(1). doi:10.3390/pharmaceutics14010105
35. Rehman A, Jafari SM, Tong Q, et al. Drug nanodelivery systems based on natural polysaccharides against different diseases. *Adv Colloid Interface Sci*. 2020;2020:284.
36. Mattheolabakis G, Milane L, Singh A, Amiji MM. Hyaluronic acid targeting of CD44 for cancer therapy: from receptor biology to nanomedicine. *J Drug Targeting*. 2015;23(7–8):605–618. doi:10.3109/1061186X.2015.1052072
37. Kinugasa Y, Matsui T, Takakura N. CD44 expressed on cancer-associated fibroblasts is a functional molecule supporting the stemness and drug resistance of malignant cancer cells in the tumor microenvironment. *Stem Cells*. 2014;32(1):145–156. doi:10.1002/stem.1556
38. Kesharwani P, Chadar R, Sheikh A, Rizg WY, Safhi AY. CD44-targeted nanocarrier for cancer therapy. *Front Pharmacol*. 2021;12:800481. doi:10.3389/fphar.2021.800481
39. Chen S, Tam YYC, Lin PJC, Sung MMH, Tam YK, Cullis PR. Influence of particle size on the in vivo potency of lipid nanoparticle formulations of siRNA. *J Control Release*. 2016;235:236–244. doi:10.1016/j.jconrel.2016.05.059
40. Chen W, Wang W, Xie Z, et al. Size-dependent penetration of nanoparticles in tumor spheroids: a multidimensional and quantitative study of transcellular and paracellular pathways. *Small*. 2023;2013:1.
41. Wu J, Wang F, Dong J, et al. Therapeutic response of multifunctional lipid and micelle formulation in hepatocellular carcinoma. *ACS Appl Mater Interfaces*. 2022;14(40):45110–45123. doi:10.1021/acsami.2c10446
42. Pretor S, Bartels J, Lorenz T, et al. Cellular uptake of coumarin-6 under microfluidic conditions into HCE-T cells from nanoscale formulations. *Mol Pharm*. 2015;12(1):34–45. doi:10.1021/mp500401t
43. Finke JH, Richter C, Gothsch T, et al. Coumarin 6 as a fluorescent model drug: how to identify properties of lipid colloidal drug delivery systems via fluorescence spectroscopy? *Eur J Lipid Sci Technol*. 2014;116(9):1234–1246. doi:10.1002/ejlt.201300413
44. Kalli M, Poskus MD, Stylianopoulos T, Zervantonakis IK. Beyond matrix stiffness: targeting force-induced cancer drug resistance. *Trends Cancer*. 2023;9(11):937–954. doi:10.1016/j.trecan.2023.07.006
45. Najafi M, Farhood B, Mortezaee K. Extracellular matrix (ECM) stiffness and degradation as cancer drivers. *J Cell Biochem*. 2019;120(3):2782–2790. doi:10.1002/jcb.27681
46. Li M, Sun J, Zhang W, Zhao Y, Zhang S, Zhang S. Drug delivery systems based on CD44-targeted glycosaminoglycans for cancer therapy. *Carbohydr Polym*. 2021;251:117103. doi:10.1016/j.carbpol.2020.117103
47. Zhang M, Ma Y, Wang Z, et al. A CD44-targeting programmable drug delivery system for enhancing and sensitizing chemotherapy to drug-resistant cancer. *ACS Appl Mater Interfaces*. 2019;11(6):5851–5861. doi:10.1021/acsami.8b19798
48. Wen C, Wu L, Fu L, Zhang X, Zhou H. Berberine enhances the anti-tumor activity of tamoxifen in drug-sensitive MCF-7 and drug-resistant MCF-7/TAM cells. *Mol Med Rep*. 2016;14(3):2250–2256. doi:10.3892/mmr.2016.5490
49. Chen G, Deng S, Liu S, et al. pH and ROS dual-sensitive nanocarriers for the targeted co-delivery and on-demand sequential release of tofacitinib and glucosamine for synergistic rheumatoid arthritis treatment. *Small*;2024. e2308520. doi:10.1002/smll.202308520
50. Jin MZ, Jin WL. The updated landscape of tumor microenvironment and drug repurposing. *Signal Transduct Target Ther*. 2020;5(1):166. doi:10.1038/s41392-020-00280-x
51. Deepak KGK, Vempati R, Nagaraju GP, et al. Tumor microenvironment: challenges and opportunities in targeting metastasis of triple negative breast cancer. *Pharmacol Res*. 2020;153:104683. doi:10.1016/j.phrs.2020.104683
52. Li YJ, Wu JY, Hu XB, Ding T, Tang T, Xiang DX. Biomimetic liposome with surface-bound elastase for enhanced tumor penetration and chemo-immumotherapy. *Adv Healthcare Mater*. 2021;10(19). doi:10.1002/adhm.202100794
53. Henke E, Nandigama R, Ergün S, Bassell GJ, Mihailescu MR. Extracellular matrix in the tumor microenvironment and its impact on cancer therapy. *Front Mol Biosci*. 2020;7:6. doi:10.3389/fmolb.2020.00006

54. Geng X, Chen H, Zhao L, et al. Cancer-associated fibroblast (CAF) heterogeneity and targeting therapy of cafs in pancreatic cancer. *Front Cell Dev Biol*. 2021;9:655152. doi:10.3389/fcell.2021.655152
55. Akanda MR, Ahn EJ, Kim YJ, et al. Different expression and clinical implications of cancer-associated fibroblast (CAF) markers in brain metastases. *J Cancer*. 2023;14(3):464–479. doi:10.7150/jca.80115
56. Figueiredo CC, Pereira NB, Pereira LX, et al. Double immunofluorescence labeling for CD31 and CD105 as a marker for polyether polyurethane-induced angiogenesis in mice. *Hist Histopathol*. 2019;34(3):257–264. doi:10.14670/HH-18-038